RESEARCH   **Open Access**

Biologically-inspired data decorrelation for hyper-spectral imaging

Artzai Picon[1*], Ovidiu Ghita[2], Sergio Rodriguez-Vaamonde[1], Pedro Ma Iriondo[3] and Paul F Whelan[2]

Abstract

Hyper-spectral data allows the construction of more robust statistical models to sample the material properties than the standard tri-chromatic color representation. However, because of the large dimensionality and complexity of the hyper-spectral data, the extraction of robust features (image descriptors) is not a trivial issue. Thus, to facilitate efficient feature extraction, decorrelation techniques are commonly applied to reduce the dimensionality of the hyper-spectral data with the aim of generating compact and highly discriminative image descriptors. Current methodologies for data decorrelation such as principal component analysis (PCA), linear discriminant analysis (LDA), wavelet decomposition (WD), or band selection methods require complex and subjective training procedures and in addition the compressed spectral information is not directly related to the physical (spectral) characteristics associated with the analyzed materials. The major objective of this article is to introduce and evaluate a new data decorrelation methodology using an approach that closely emulates the human vision. The proposed data decorrelation scheme has been employed to optimally minimize the amount of redundant information contained in the highly correlated hyper-spectral bands and has been comprehensively evaluated in the context of non-ferrous material classification

Keywords: Hyper-spectral data, feature extraction, fuzzy sets, material classification

1. Introduction

Hyper-spectral imaging involves the acquisition (see Figure 1) and interpretation of multi-dimensional digital images that are able to sample the spectral properties of the materials associated with the visualized objects [1]. Nowadays, the current range of spectral imaging systems is able to capture multiple bands from ultraviolet to far infrared with good bandwidth resolution. This increased flexibility in the image acquisition process prompted the inclusion of the hyper-spectral imaging systems in the development of a wide variety of computer vision systems, such as video surveillance, food inspection, medical imaging, remote sensing, and material classification [2-4].

The main characteristic of the hyper-spectral images is that each pixel is defined by a multi-dimensional vector whose elements are the spectral (electromagnetic or wavelengths) components that are captured from the light arriving at the spectral sensor. In this regard, the

hyper-spectral imaging sensors (or spectrographs) allow the extraction of a richer source of information beyond the visible spectral domain (that is usually captured by a standard color camera), a fact that opens the possibility to analyze not only the tri-chromatic characteristics of the scene materials, but also their chemical composition [1,3,5-7].

One issue that is common for all hyper-spectral applications is associated with the optimal evaluation of the material characteristics in the hyper-spectral domain. To address this issue, several distance metrics that evaluate the dissimilarity among the spectral descriptors extracted from the analyzed materials were proposed in the specialized literature [8,9]. One apparent conclusion that emerged from past investigations indicates that classical approaches that evaluate the distance between unprocessed hyper-spectral features in the multi-dimensional Euclidean, space or those based on the measurement of the angle between spectrums' SAM (spectral angle mapper) [9-11] provide information in regard to the similarity between two or more materials, but they are not able to overcome the high correlation associated

* Correspondence: artzai.picon@tecnalia.com
[1]Information and Interaction Systems Unit, Tecnalia, Zamudio, Bizkaia, Spain
Full list of author information is available at the end of the article

Figure 1 The principle of the hyper-spectral image acquisition process.
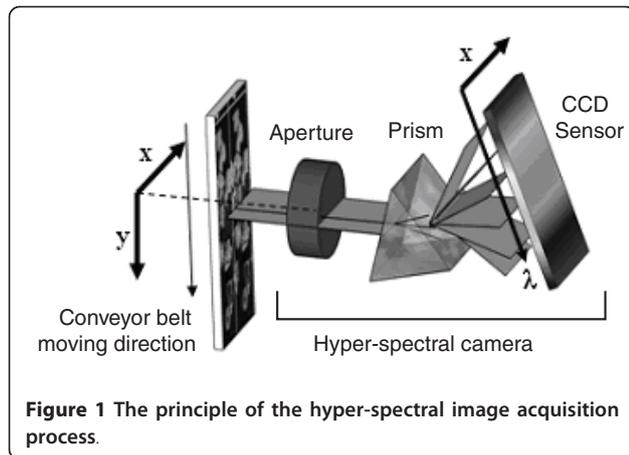
with the hyper-spectral descriptors [3]. This observation is in particular valid, as the simplistic analysis of the raw hyper-spectral data is inappropriate for several practical reasons. The first reason is given by the fact that the analysis of the unprocessed hyper-spectral data is computationally intensive, while the second reason is associated with the high correlation attained by the closely spaced spectral bands in the hyper-spectral domain [12]. These factors substantially complicate the material classification process as the increased spectral correlation reduces the discriminative power associated with the spectral descriptors that describe the properties of the analyzed materials. This problem is known as the Hughes phenomenon [12,13] and states that the number of samples required to train a specific classifier increases exponentially with the increase in the number of spectral features [12,13].

The intra-class variations for each analyzed material can be better modeled if the high dimensionality of the hyper-spectral data is reduced before feature extraction. In this sense, to circumvent the problems caused by the large feature vectors calculated from raw (unprocessed) hyper-spectral data when used for classification purposes, feature reduction (or decorrelation) techniques are usually applied to avoid the Hughes phenomenon [12-14]. Thus, the hyper-spectral data has been commonly subjected to standard decorrelation schemes, such as PCA, WD [15-19], uniform band design (UBD) [20] or its dimensionality reduced by applying methods based on user-defined band selection (UDBS) [21-23]. Nonetheless, these classic decorrelation techniques reduce the number of features calculated from the hyper-spectral spectrum, but it is useful to note that these data transformations often alter the physical meaning of the extracted features, and as a result they are difficult to interpret and analyze. In addition to this, the above-mentioned techniques involve tedious and subjective training procedures that are applied to sample

the distributions associated with all materials to be analyzed. The requirement of laborious training procedures pose a particular challenge when developing flexible industrial applications and this issue is substantially exacerbated if new materials are often included in the classification process, a situation when retraining is necessary.

To avoid these problems, more flexible methodologies that are able to perform hyper-spectral data decorrelation have to be devised. These approaches should reduce the dimensionality of the hyper-spectral data by selecting the most relevant bands that maximize the classification rate (or the separation among materials) without reducing the discriminative power of the extracted features [24]. To achieve these goals, branch and bound algorithms [25], machine learning techniques based on genetic algorithms [26], and methods based on the evaluation of the data using a combination of classifiers [27] were recently proposed. These methods proved efficient when applied to extract the discriminative features that characterize the materials included in the datasets, but similar to classic decorrelation approaches, they entail retraining if the automatic sorting system requires the inclusion of new materials in the classification process. Given these limitations, an optimal decorrelation technique should comply with the following set of assumptions:

- To reduce as much as possible the dimensionality of the hyper-spectral data.
- To maximize the discriminative power of the decorrelated feature vectors.
- Should not be dependent on training procedures, so they can be used when new materials are included in the classification process.
- Data decorrelation should not alter the physical meanings of the transformed spectral components.
- Data decorrelation should be material independent.

To accommodate these requirements, in this article we propose a new data decorrelation scheme using an approach that is closely related to that employed by the human visual system (HVS) in the process of converting the electromagnetic radiation that is emitted by the surrounding objects into chromatic information. The main contribution associated with this study resides in the application of the fuzzy sets theory, as introduced by Zadeh [28], to maximize the discriminative power associated with the hyper-spectral features calculated for each pixel in the image. Other contributions resulting from our study are located in the detailed evaluation of the proposed data decorrelation technique when applied to non-ferrous material classification tasks.

This article is organized as follows: Section 2 introduces the proposed hyper-spectral data decorrelation technique, where the main emphasis is placed on the extension of the biologically inspired models when applied to the hyper-spectral domain. Section 3 details the experimental results, while concluding remarks are provided in Section 4.

2. Biologically-inspired hyper-spectral modeling

The HVS has adapted through years of evolution to efficiently capture the visual information that helps the humans in the process of interacting with the surrounding environment. The human eye is able to capture the electromagnetic spectrum in the range 400-700 nm, although other animals like fish or insects can acquire information from the UV spectrum as well.

The photoreceptors present in the human eye consist of three different types of spectral-sensitive cells, where each cell (retinal cone) is able to convert the electromagnetic information into chromatic information [29]. Each of these visual receptors, as shown in Figure 2, responds strongly to restricted domains of the electromagnetic spectrum (S = blue, M = green, L = red) and the first stage of human color information entails a decorrelation process that evaluates the response generated by each type of photoreceptor. As indicated by several studies that investigated the HVS with respect to the chromatic perception [29-32], the sensitivity of the human eye employs models that are consistent with the fuzzy sets theory (see Figure 2).

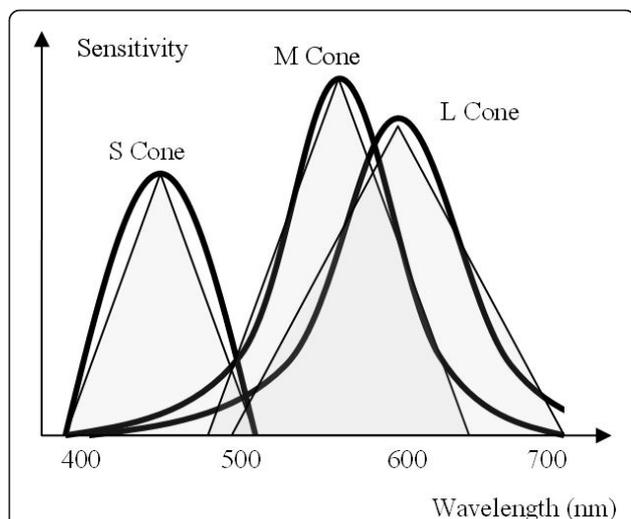Following this theory, in this article we propose a new data decorrelation approach where each defined fuzzyset

would correspond to a "virtual retinal cone" that responds strongly at specific wavelengths of the hyper-spectral domain using models that are consistent with the human chromatic perception. More precisely, the proposed approach can be conceptualized as an *hyper-spectral eye*, where each fuzzyset emulates the spectral response of a distinct type of retinal receptor in a restricted bandwidth of the hyper-spectral domain.

The proposed data decorrelation method exploits the knowledge that the adjacent wavelengths of the spectrum are more correlated than the more distant wavelengths. This observation is justified since the electromagnetic spectra emitted by solid materials show a slow variation with respect to successive wavelengths. As a result of this coherent radiometric model, the spectral information can be better sampled by groups of continuously distributed wavelengths rather than unique spectral bands, which is the case of the unprocessed (raw) hyper-spectral data. To achieve this, the response for each "virtual" (fuzzy) cone is calculated as the sum of the weighted intensity values corresponding to a sub-domain of adjacent wavelengths, and in this process the spectrum is divided into a predefined number of distinct groups to attain the desired spectral selectivity. Nonetheless, the quantization of the spectral response will be problematic at the interface between consecutive sub-domains and to avoid the issues that are caused by a crisp division of the spectrum, in this article a method based on the spectrum fuzzyfication is proposed. This involves the separation of the hyper-spectral data into a predefined number of fuzzy groups, where each group covers a range of wavelengths and the contribution of each wavelength is modeled by fuzzy membership rules.

Let **L** be the N-dimensional spectral vector as defined in Eq. 1 and M be the number of fuzzysets that cover the full hyper-spectral domain.

$$\mathbf{L} = \{L_1, L_2, ..., L_N\}^T \qquad (1)$$

To sample the spectral response, a membership function is defined to measure the level of appartenance for any wavelength of the spectrum to its related fuzzysets. For the sake of simplicity, the membership functions are commonly implemented either as triangular shaped (Eq. 2) or Gaussian functions (Eq. 3).

$$Mf_k(\lambda) = \begin{cases} 1 - \left| \dfrac{\lambda - \lambda_{Ck}}{D} \right|, & \lambda_{Ck} - D < \lambda < \lambda_{Ck} + D \\ 0, & \text{Otherwise} \end{cases} \qquad (2)$$

$$Mf_k(\lambda) = \left(\frac{1}{2\pi\sigma^2} \right)^{\frac{1}{2}} e^{-\frac{1}{2\sigma^2}(\lambda - \lambda_{Ck})^2} \qquad (3)$$

Figure 2 Sensitivity of the human visual receptors to the different wavelengths of the spectrum. In this diagram, for simplicity reasons, the sensitivity of the human receptors is modeled by triangular-shaped fuzzysets.

Where λ_{Ck} is the central wavelength value of the fuzzyset $k \in [1,M]$ and D defines the spectral separation between two consecutive central wavelengths when triangular shaped functions are employed. If the membership functions are modeled using Gaussian distributions, the standard deviation σ in Eq. 3 plays the role of the parameter D in Eq. 2. In practice the triangular shaped functions are preferred, since they model linearly the grade of membership of the wavelengths contained in each fuzzyset with respect to the central wavelength and this approach is also followed in the implementation detailed in this article. Figure 3 provides a graphical representation of the triangular membership functions when applied for spectrum fuzzyfication.

As illustrated in Figure 3, each of the spectrum's wavelengths (λ_i, $I \in [1,N]$) has a membership grade different than zero for the two fuzzysets that intersect it and a membership grade of zero for the rest of the fuzzysets, a process that is similar with the chromatic perception process performed by the human eye's visual receptors. As mentioned earlier, our approach emulates the principles associated with the human chromatic perception to the hyper-spectral domain and this process is illustrated in Figure 4.

The decorrelated data are calculated for each pixel in the image and consists in an M-dimensional vector, where for each fuzzyset with the central wavelength λ_{Ck} ($k \in [1,M]$) an energy value E_k is calculated by weighing the intensity of each wavelength of the spectrum λ_i($i \in [1,N]$) with respect to the membership function as follows,

$$E_k = \int_{\lambda=1}^{\lambda=N} Mf_k(\lambda) \cdot L(\lambda) d\lambda \qquad (4)$$

where the energy E_k defined in Eq. 4 measures the strength of the intensity signal captured by the hyper-

Figure 4 An example that illustrates the membership grade associated with the wavelength λ_i.
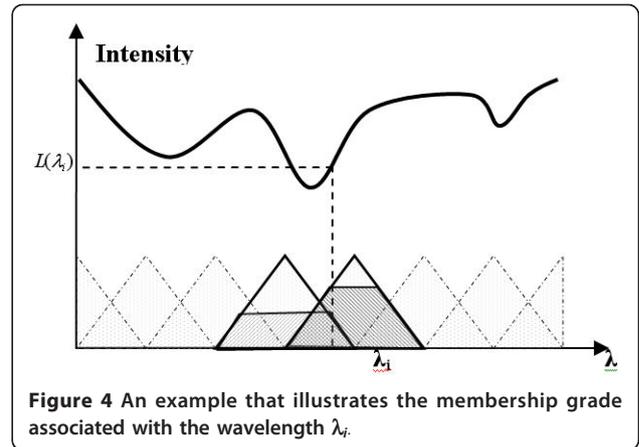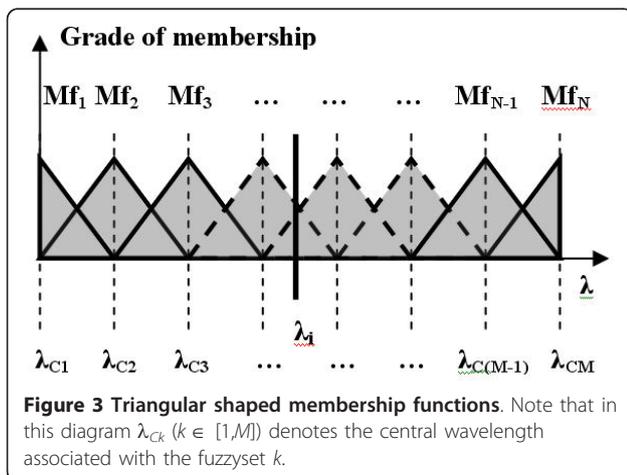
spectral camera within the bandwidth covered by the fuzzyset with the index k. Based on the values of energies calculated for each of the M fuzzysets, we can attain useful information that describes the radiometric (or spectral) properties of the scene materials that were captured during the hyper-spectral image acquisition process. As indicated earlier, each hyper-spectral pixel (or hyper-spectral feature) is defined by a vector containing the energy values E_k ($k \in [1,M]$) as shown in Eq. 5.

$$\mathbf{X} = \{E_1, E_2, ..., E_M\}^T \qquad (5)$$

Since the light absorption for a particular material is selective for a well-defined range of wavelengths, this makes the analysis of the spectral energies calculated using Eq. 4 adequate and allows us to derive more accurate hyper-spectral features, whose discriminative power is increased when compared to the features calculated from the unprocessed data. At the same time, since the calculation of the energies for all fuzzysets involves a local summation modulated by the membership function, this approach has another obvious advantage as it performs a drastic reduction of the image noise present in the unprocessed (raw) hyper-spectral data. In this manner, the absorption bands that are characteristic for each material are directly parameterized by the energy calculated for each fuzzyset.

This fuzzy representation facilitates the analysis of the spectral information in an efficient manner by addressing all conditions that were mentioned in the last part of the introductory section. In this regard, the proposed data decorrelation scheme based on the spectrum fuzzyfication does not involve any training procedures as those required by other decorrelation techniques, such as PCA, LDA, WD, or UDBS. In addition to this, the proposed technique allows the extraction of the spectral features that are strongly related to the radiometric properties of the analyzed materials and the dimensionality of the hyper-spectral data is optimally reduced


Figure 3 Triangular shaped membership functions. Note that in this diagram λ_{Ck} ($k \in [1,M]$) denotes the central wavelength associated with the fuzzyset k.

since the fuzzyfication procedure maximizes the decorrelation between adjacent spectral bands.

3. Application to non-ferrous material classification

As indicated in the previous section, the proposed data decorrelation scheme based on spectrum fuzzyfication implements an efficient dimensionality reduction of the unprocessed hyper-spectral data by sampling the most discriminative characteristics of the spectral bands that measure the radiometric properties of the materials included in the classification process. In order to evaluate the efficiency of the proposed technique, in this section we compare its performance against those attained by different decorrelation schemes in the context of non-ferrous material classification.

To evaluate the efficiency of the analyzed decorrelation methods, in our study we have used sample spectra that are acquired for three different non-ferrous materials (see Figure 5). Among them, the materials A and C present are significant spectral similarities, while the material B is the most dissimilar.

In this initial study, we aim to evaluate the performance of the analyzed decorrelation schemes by quantifying the separability that is measured as the distance between the non-ferrous samples used in our experimental set-up. To achieve this N_2 collections of four spectral samples were used for experimentation, two of them belonging to the material A (aluminum) (A_1 and A_2) and the other two belonging to the materials B (copper) and C (stainless steel), respectively. In each collection, the separability has been estimated by measuring the intra- and inter-class distances as shown in Eq. 6.

Figure 5 Sample spectrums calculated for materials A, B, and C.
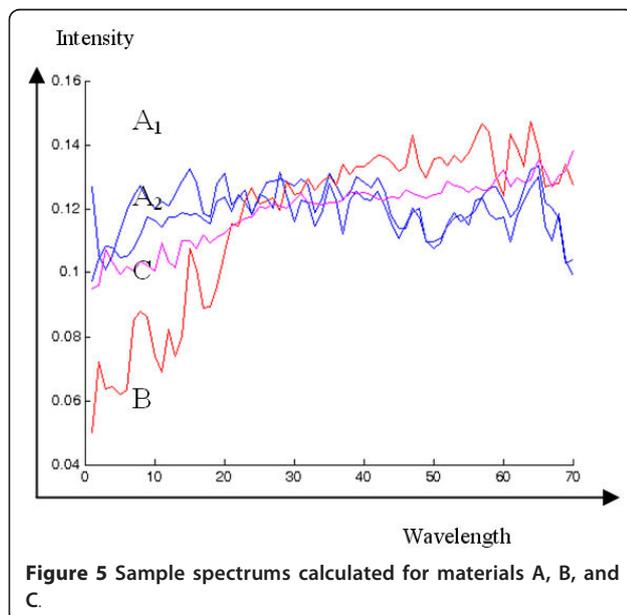
$$\text{Separability} = \frac{\sum_{i=1}^{N_2} \dfrac{Dist(A_{1_i}, B_i) + Dist(A_{1_i}, C_i)}{2Dist(A_{1_i}, A_{2_i})}}{N_2} \quad (6)$$

When evaluating the separability between the non-ferrous spectrums (A, B and C materials) an important issue is the selection of the distance metric. To provide a comprehensive evaluation, in our study the differences between the hyper-spectral feature vectors are quantified using classical metrics that were widely used in the development of hyper-spectral classification schemes. In this regard, metrics like Manhattan, Tchebychev, and Euclidean distances are used as well as other metrics, such as SAM [10,11] (SAM is also referred in the literature to as goodness of fit coefficient (GFC) [9]) and probabilistic metrics like spectral information divergence (SID) [3] (see Eqs. 7, 8).

$$\cos(\alpha) = \frac{\langle L_a, L_b \rangle}{\|L_a\| \, \|L_b\|}, \; SAM(L_a, L_b) = \cos^{-1}(\alpha) \quad (7)$$

$$SID(L_a, L_b) = D_{KL}(L_a, L_b) + D_{KL}(L_b, L_a) \quad (8)$$

where L_a and L_b are the hyper-spectral vectors, <. > is the scalar product, ||.|| defines the standard L_2 vector norm and D_{KL} denotes the Kullback-Leibler divergence.

Table 1A depicts the results obtained when the feature vectors are extracted from the hyper-spectral data that has been subjected to various decorrelation schemes. In these tests, the separability (calculated using Eq. 6) achieved when the feature vectors are calculated from

Table 1 (A) Separability achieved by the analyzed data decorrelation techniques (absolute values) and (B) Separability achieved by the analyzed data decorrelation techniques (z-score normalized values)

	RAW	PCA	LDA	WD	UDBS	UBD	FuzzySets
A							
City block distance	237.2	132.2	121.0	334.7	262.7	306.4	359.7
Euclidean distance	222.4	134.7	143.5	305.5	258.9	313.6	362.7
Tchebychev distance	136.9	181.3	190.6	277.3	270.9	299.5	370.5
SAM	100.8	253.7	151.0	12.8	173.7	39.6	101.1
SID	421.5	182.9	119.7	187.1	320.8	355.9	782.4
B							
City block distance	-0.14	-1.26	-1.38	0.89	0.13	0.59	1.16
Euclidean distance	-0.30	-1.31	-1.21	0.65	0.12	0.75	1.31
Tchebychev distance	-1.36	-0.81	-0.69	0.38	0.30	0.65	1.53
SAM	-0.22	1.64	0.39	-1.29	0.67	-0.97	-0.22
SID	0.37	-0.70	-0.98	-0.68	-0.08	0.08	1.99

raw (unprocessed) hyper-spectral data is compared against the separability obtained where a range of data decorrelation methods (such as PCA, LDA, WD [18], UBD [20], UDBS [23], and the proposed fuzzysets-based method) are applied before feature extraction. Since the results reported for the various distance metrics in Table 1A have different units and limits of variation, to allow a direct comparison they are normalized to a common scale by using z-scores to attain zero mean and unit variance normalized results (i.e., standard variables). The z-score normalized results are depicted in Table 1B.

The experimental results shown in Table 1A, B indicate that the proposed fuzzyset method outperforms the other analyzed techniques for all distance metrics with the exception of SAM, where the decorrelation schemes based on PCA, LDA, and UBD achieved better performance. These results are motivated by the fact that the SAM metric samples the variation in the orientation between hyper-spectral vectors and it does not explicitly measure the closeness in the hyper-spectral domain between the extracted feature vectors. However, it is useful to mention that the increase in separability is not sufficient to fully characterize the performance of the decorrelation techniques, but the preliminary results shown in Table 1A, B give an indication that the proposed technique produced more consistent results when compared to those achieved by the classic decorrelation schemes. To fully evaluate the performance of the decorrelation methodologies analyzed in this investigation, the results shown in Table 1A, B will be complemented with the results achieved when the data decorrelation algorithms are evaluated in the context of material classification.

To attain this objective, we have developed a classification framework (see Figure 6) that consists of the following computational stages:

1) Image acquisition.
2) Hyper-spectral data normalization. This step is applied to alleviate the high spectra variability induced by shadows and various level of oxidization between samples of non-ferrous materials that are included in the same class.
3) Spectral decorrelation and extraction of the hyper-spectral feature vectors.
4) Statistical classification using a multivariate Gaussian classifier. In this approach, a Gaussian model is created for each non-ferrous material where μ and Σ are the mean vector and the covariance matrix, respectively, of the modeled material class. The classification process is implemented using Eq. 9, where X is the feature vector associated with the unknown (to be classified) non-ferrous material.
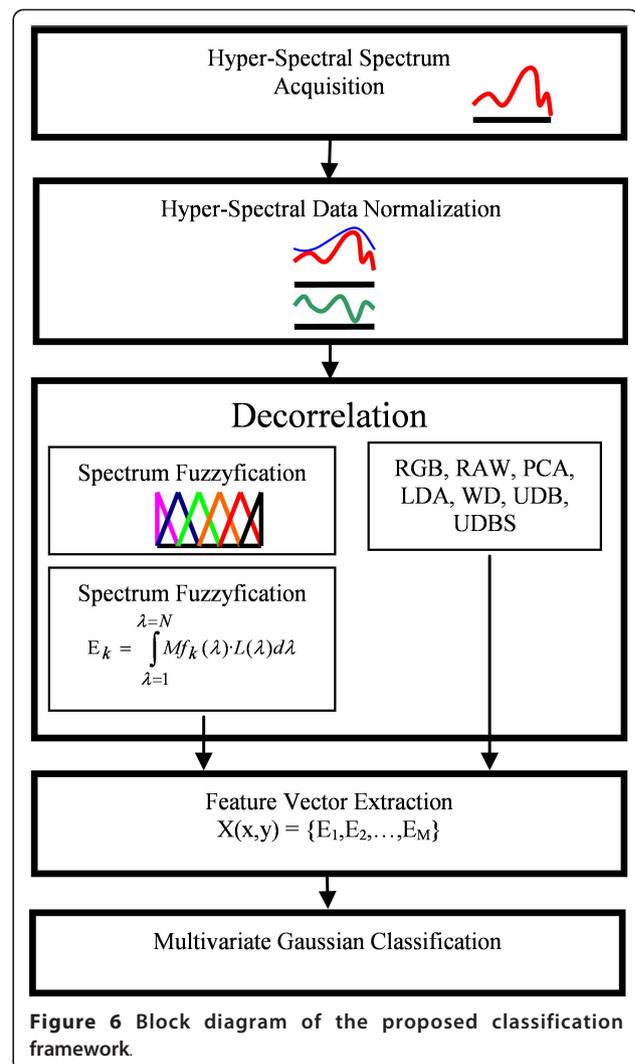

Figure 6 Block diagram of the proposed classification framework.

$$N(X| \ \mu, \sum) = \frac{1}{(2 \cdot \pi)^{M/2}} \frac{1}{|\sum|^{1/2}} e^{\left\{-\frac{1}{2}(x-\mu)^T \sum^{-1}(x-\mu)\right\}} \quad (9)$$

As mentioned earlier, we elected to assess the performance of the proposed decorrelation technique (spectrum fuzzyfication) in the context of material classification. This approach is motivated by the fact that the non-ferrous materials present similar spectral properties and their robust classification pose a challenging research issue. In this investigation the following materials were used for experimentation: white copper, aluminum, stainless steel, brass, copper, and lead (see Figure 7).

In the experimental analysis, half of the data was used for training and the remaining half was used for testing. From each of these datasets more than 500,000 hyper-spectral vectors were extracted. As indicated before, the non-ferrous materials present substantial similarities in
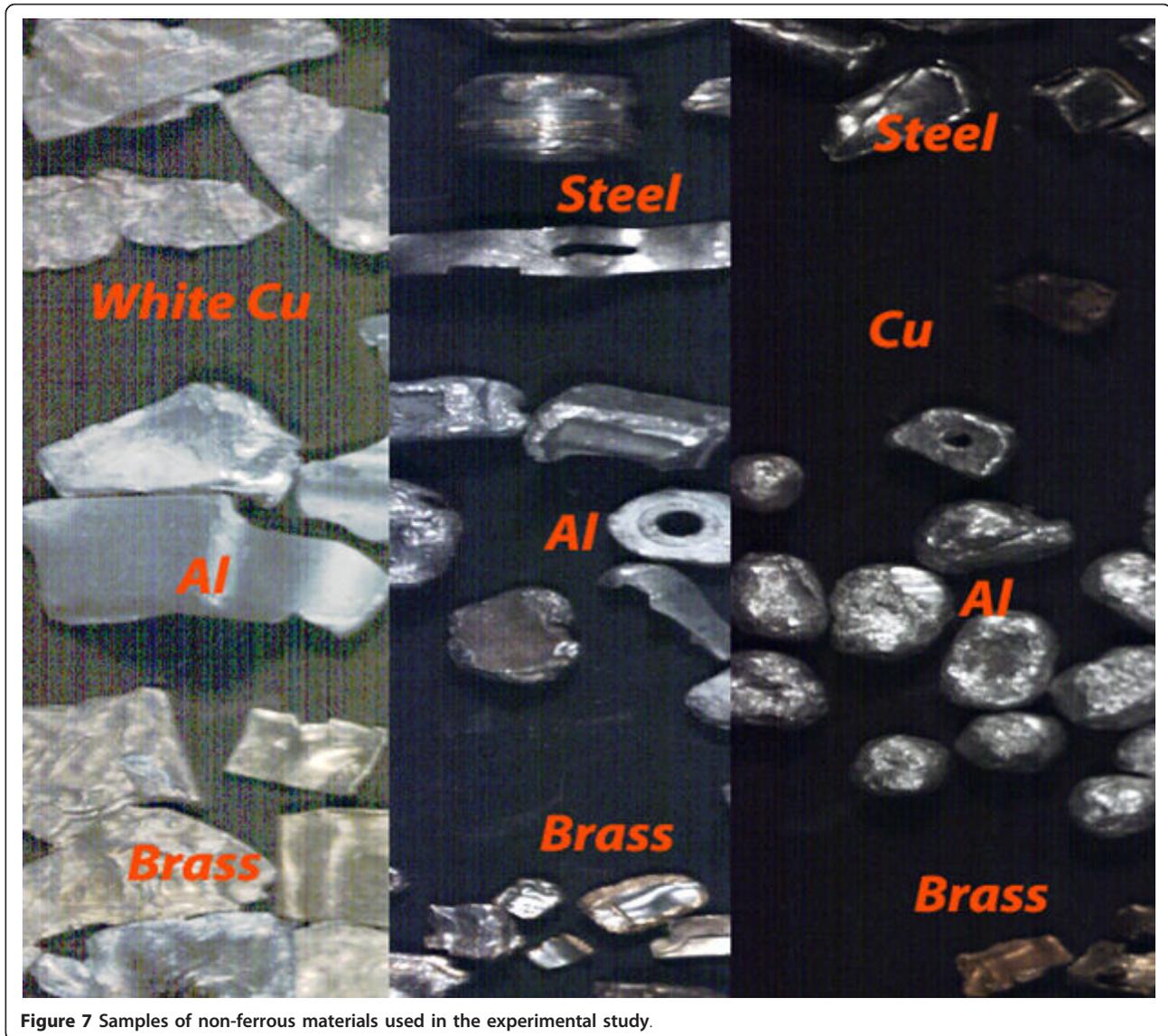
Figure 7 Samples of non-ferrous materials used in the experimental study.

their chromatic appearance, and in addition it is useful to note that their spectra modeled from unprocessed hyper-spectral data show considerable intra-class dispersion and a relative high inter-class similarity (see Figure 8), a fact that makes their classification particularly difficult. Nonetheless, these intrinsic properties of the non-ferrous materials generate a challenging classification scenario that would allow a comprehensive performance evaluation for the classic and proposed decorrelation techniques.
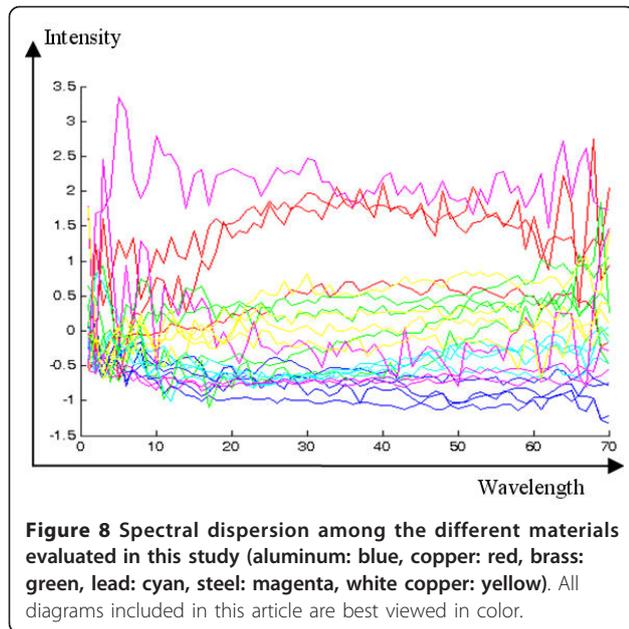
3.1. Hyper-spectral data normalization

Due to the wide variety of shapes associated with the shredded non-ferrous materials (see Figure 7), their arbitrary orientations on the conveyor belt and imperfections in the optical and sensing equipment, the hyper-

spectral image acquisition process is affected by the shadows, specular reflections (highlights), and inhomogeneous illumination. To compensate for these image formation issues, in our investigation two data normalization schemes, that were proposed by Stockman and Gevers [33] (see Eq. 10) and Montoliu et al [34] (see Eq. 11) were investigated.

$$L_{normS}(\lambda_j) = L_n(\lambda_j) - \min_{i \in [1,N]} \left(L_n(\lambda_i) \right) \tag{10}$$

$$L_{normM}(\lambda_j) = \frac{L(\lambda_j) - \min_{i \in [1,N]} \left(L(\lambda_i) \right)}{\sum_{n=1}^{N} \left(L(\lambda_n) - \min_{i \in [1,N]} \left(L(\lambda_i) \right) \right)} \tag{11}$$

Figure 8 Spectral dispersion among the different materials evaluated in this study (aluminum: blue, copper: red, brass: green, lead: cyan, steel: magenta, white copper: yellow). All diagrams included in this article are best viewed in color.

where $L_n(\lambda_j) = \dfrac{L(\lambda_j)}{\sum_{n=1}^{N} L(\lambda_n)}$ and $j \in [1, N]$.

The experimental results shown in Table 2 indicate that both methods reduce to some extent the undesired effects generated by shadows, highlights and uneven illumination, and Figure 9 illustrates the performance of the investigated intensity correction algorithms when applied to a hyper-spectral image consisting of a cluttered arrangement of non-ferrous materials. Since the method proposed by Stockman and Gevers [33] returns better performance, the classification results that will be reported in the next section are obtained when the hyper-spectral data are normalized using this approach.

3.2. Classification results
The efficiency of the features extracted after the application of the decorrelation techniques is evaluated by creating a Gaussian model for each non-ferrous material using the expression shown in Eq. 9. Table 3 illustrates

Table 2 The effect of the intensity correction on the classification results

Normalization method

Decorrelation technique	No correction (%)	Stockman (%)	Montoliu (%)
Fuzzy sets ($M = 8$)	53.45	71.52	60.29
Fuzzy sets ($M = 4$)	49.13	63.10	55.62
PCA ($M = 8$)	44.58	66.43	57.63
LDA	48.04	62.86	44.36
WD	61.25	63.79	60.29
RGB	25.14	43.83	44.54
RAW	20.62	55.67	39.85

the classification performance obtained when the RAW, RGB, and decorrelated hyper-spectral data (PCA, LDA, WD, UBD, UDBS, and the proposed technique) are used for non-ferrous material classification.

The results shown in Table 3 indicate that the RGB data, as expected, returns the worst performance (43.83%), and better results are obtained when unprocessed (raw) hyper-spectral information is used for material classification (55.67%). However, the experimental data clearly indicate that the application of decorrelation techniques improve significantly the classification results and the results reported in Table 3 reveal that the proposed technique outperforms the classic decorrelation schemes including PCA, LDA, Wavelet, and UBD. For the sake of completeness, results are also reported when the number of fuzzysets and the number of principal components retained after the application of PCA is varied (see Table 3). These results clearly indicate the superiority of the proposed decorrelation scheme over classic algorithms based on LDA and PCA decomposition, and it is useful to note that the proposed scheme also circumvents the complications associated with the implementation of cumbersome and subjective training procedures.

4. Conclusions
In this article we introduced a new hyper-spectral decorrelation methodology that has been specifically designed to improve the classification accuracy of the non-ferrous material sorting process. While the primary aim of this article was focused on the development of a decorrelation approach that is able to optimally sample the spectral characteristics of the non-ferrous materials, in our investigation we had to confront additional issues generated by the image formation process (such as shadows, specular reflections, and inhomogeneous illumination) and practical issues related to the optimal size of the hyper-spectral feature vector.

The decorrelation approach presented in this article extends to the hyper-spectral domain, the concepts associated with the chromatic perception process performed by the human eye. In this regard, the developed scheme applied the fuzzy sets theory to decorrelate the high-dimensional hyper-spectral images based on the knowledge that the data encompassed by closely spaced wavelengths in the spectral domain is more correlated than the information provided by more distant wavelengths. The proposed decorrelation scheme does not require any training procedure to extract the most relevant features and this is another important advantage that our approach has over other classic data decorrelation techniques.

In our study, the performance of the data decorrelation approach detailed in this article has been
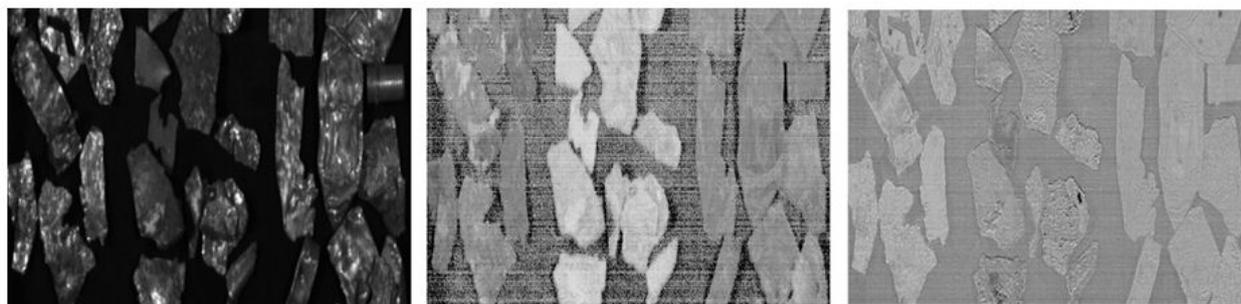
Figure 9 Results achieved after the application of intensity correction. **(a)** Raw hyper-spectral data. **(b)** Stockman and Gevers [33] intensity correction. **(c)** Montoliu et al [34] intensity correction.

Table 3 Non-ferrous material classification results (Stockman and Gevers [33] intensity correction)

NUMBER OF FEATURES (M)	RAW	PCA (%)	LDA	WD (%)
2		53.08		51.05
4		61.40		53.96
8		66.43	62.86	63.79
16		64.11		69.59
24		67.95		68.69
80	55.67			
	UDBS	UBD	Fuzzy sets	RGB
2	47.02%	48.82%	52.76%	43.83%
4	59.75%	57.22%	63.10%	
8	66.63%	66.06%	71.52%	
16	64.58%	66.24%	71.43%	
24	67.25%	66.72%	71.67%	
80				

numerically evaluated against a wide range of classic decorrelation schemes and the experimental results indicate that the proposed method outperforms the classic techniques with respect to class separability and when applied to material classification tasks. In our future investigations we will focus on the deployment of the proposed hyper-spectral decorrelation scheme into practical systems that are developed for robust material classification.

Abbreviations
GFC: goodness of fit coefficient; HVS: human visual system; LDA: linear discriminant analysis; PCA: principal component analysis; SAM: spectral angle mapper; SID: spectral information divergence; UBD: uniform band design; UDBS: user-defined band selection; WD: wavelet decomposition.

Author details
[1]Information and Interaction Systems Unit, Tecnalia, Zamudio, Bizkaia, Spain [2]Centre for Image Processing and Analysis, Dublin City University, School of Electronic Engineering, Glasnevin, Dublin 9, Ireland [3]Department of Automatic Control and Systems Engineering, University of the Basque Country UPV-EHU, Spain

References
1. H Grahn, P Geladi, (eds.), *Techniques and Applications of Hyperspectral Image Analysis*. (Wiley, Chichester, 2007) ISBN-10: 0-470-01086-X
2. DA Wahab, A Hussain, E Scavino, M Mustafa, H Basri, Development of a prototype automated sorting system for plastic recycling. Am J Appl Sci. **3**, 1924–1928 (2006)
3. CI Chang, *Hyperspectral Imaging: Techniques for Spectral Detection and Classification* (Kluwer Academic Publishers Group, New York, 2003) ISBN:0-306-47483-5
4. B Tso, RC Olsen, Scene Classification Using Combined Spectral, Textural and Contextual Information. In *Algorithms and Technologies for Multispectral, Hyperspectral, and Ultraspectral Imagery* X (SPIE, 2004)
5. Specim Spectral Imaging Ltd, http://www.specim.fi/. Accessed 27th Aug 2009
6. D Slater, G Healey, Material classification for 3D objects in aerial hyperspectral images, in *IEEE Computer Society Conference on Computer Vision and Pattern Recognition (CVPR'99)*, **2**, 2262–2267 (1999)
7. G Healey, D Slater, Models and methods for automated material identification in hyperspectral imagery acquired under unknown illumination and atmospheric conditions. IEEE Trans Geosci Remote Sens. **37**, 2706–2717 (1999). doi:10.1109/36.803418
8. N Keshava, Distance metrics and band selection in hyperspectral processing with application to material classification and spectral libraries. IEEE Trans Geosci Remote Sens. **42**, 1552–1565 (2004)
9. FH Imai, MR Rosen, RS Berns, Comparative Study of Metrics for Spectral Match Quality, in *Proc of the First European Conference on Colour in Graphics, Imaging and Vision (CGIV)*, 492–496, (2002)
10. FA Kruse, AB Lefkoff, JB Boardman, KB Heidebrecht, AT Shapiro, PJ Barloon, AF Goetz, the spectral image processing system (SIPS)–interactive visualization and analysis of imaging spectrometer data. Remote Sens Environ. **44**, 145–163 (1933)
11. J Hernández-Andrés, J Romero, LR Lee, Colorimetric and spectroradiometric characteristics of narrow-field-of-view clear skylight in Granada, Spain. J Opt Soc Am A **18**, 412–420 (2001). doi:10.1364/JOSAA.18.000412
12. H Pai-Hui, Feature extraction of hyperspectral images using wavelet and matching pursuit. ISPRS J Photogram Remote Sens. **62**, 78–92 (2007). doi:10.1016/j.isprsjprs.2006.12.004
13. GF Hughes, On the mean accuracy of statistical pattern recognizers. IEEE Trans Inf Theory. **14**, 55–63 (1968). doi:10.1109/TIT.1968.1054102

14. D Manolakis, D Marden, Dimensionality reduction of hyperspectral imaging data using local principal component transforms. In *Algorithms and Technologies for Multispectral, Hyperspectral and Ultraspectral Imagery X* (SPIE, 2004)

15. BK Feather, SA Fulkerson, JH Jones, RA Reed, M Simmons, D Swann, WE Taylor, LS Bernstein, Compression technique for plume hyperspectral images. *Algorithms and Technologies for Multispectral, Hyperspectral and Ultraspectral Imagery XI* (SPIE, 2005)

16. P Tatzer, M Wolf, T Panner, Industrial application for inline material sorting using hyperspectral imaging in the NIR range. Real-Time Imaging. Spectr Imaging II. **11**, 99–107 (2005)

17. KM Rajpoot, NM Rajpoot, Wavelet based segmentation of hyperspectral colon tissue imagery, in *7th International Multi Topic Conference* (INMIC 2003) (Islamabad, Pakistan, 2003), pp. 38–43

18. P Kempeneers, S De Backer, W Debruyn, P Coppin, P Scheunders, Generic wavelet-based hyperspectral classification applied to vegetation stress detection. IEEE Trans Geosci Remote Sens. **43**, 610–614 (2005)

19. J Wang, CI Chang, Independent component analysis-based dimensionality reduction with applications in hyperspectral image analysis. IEEE Trans Geosci Remote Sens. **44**, 1586–1600 (2006)

20. CH Lee, DA Landgrebe, Decision boundary feature extraction for non-parametic classification. IEEE Trans Syst Man Cybernet. **23**, 433–444 (1993). doi:10.1109/21.229456

21. S Perkins, K Edlund, D Esch-Mosher, D Eads, N Harvey, S Brumby, Genie pro: robust image classification using shape, texture and spectral information, in *Algorithms and Technologies for Multispectral, Hyperspectral and Ultraspectral Imagery XI* (SPIE. 2005)

22. H Kwon, SZ Der, NM Nasrabadi, H Moon, Use of hyperspectral imagery for material classification in outdoor scenes, in *SPIE Proceedings Series, Algorithms, Devices, and Systems for Optical Information Processing III*, Denver, USA. **3804**, 104–115 (1999)

23. B Guo, RI Damper, SR Gunn, JD Nelson, A fast separability based feature-selection method for high-remotely sensed image classification. Pattern Recog. **41**, 1653–1662 (2008). doi:10.1016/j.patcog.2007.11.007

24. RN Clark, GA Swayze, Mapping minerals, amorphous materials, environmental materials, vegetation, water, ice and snow, and other materials: the USGS tricorder algorithm, in *Summaries of the Fifth Annual JPL Airborne Earth Science Workshop*, ed. by Green RO (JPL Publication 95-1, 1995), pp. 39–40

25. S Nakariyakul, DP Casasent, Adaptive branch and bound algorithm for selecting optimal features. Pattern Recog Lett. **28**, 1415–1427 (2007). doi:10.1016/j.patrec.2007.02.015

26. S Yu, S De Backer, P Scheunders, Genetic feature selection combined with composite fuzzy nearest neighbor classifiers for hyperspectral satellite imagery. Pattern Recog Lett. **23**, 183–190 (2002). doi:10.1016/S0167-8655(01)00118-0

27. M Bacauskiene, A Verikas, Selecting salient features for classification based on neural network committees. Pattern Recog Lett. **25**, 1879–1891 (2004). doi:10.1016/j.patrec.2004.08.018

28. LA Zadeh, Fuzzy sets. Inf. Control. **8**, 338–353 (1965)

29. SJ Sangwine, REN Horne, *The Colour Image Processing Handbook*, (Springer, New York, 1998). ISBN 0412806207

30. A Stockman, DI MacLeod, NE Johnson, Spectral sensitivities of the human cones. J Opt Soc Am A. **10**, 2491–2521 (1993). doi:10.1364/JOSAA.10.002491

31. A Stockman, LT Sharpe, The spectral sensitivities of the middle and long-wavelength-sensitive cones derived from measurements in observers of known genotype. Vision Res. **40**, 1711–1737 (2000). doi:10.1016/S0042-6989(00)00021-3

32. E Garrote, *Algorithms for Colour Image Processing Based on Neurological Models* (PhD Thesis, University of the Basque Country, Spain. 2011)

33. R Montoliu, F Pla, AC Klaren, Illumination intensity, object geometry and highlights invariance in multispectral imaging. *Lecture Notes in Computer Science*, (Heidelberg, Germany). **3522**, 36–43 (2005). doi:10.1007/11492429_5

34. H Stockman, T Gevers, Detection and classification of hyper-spectral edges, in *Proc of the 10th British Machine Vision Conference* (1999), pp. 643–651